Reaction of Hydrogen Atoms with Hydroxide Ions in High-Temperature and High-Pressure Water†

Timothy W. Marin‡ and Charles D. Jonah

Chemistry Division, Argonne National Laboratory, Argonne, Illinois 60439

David M. Bartels*

Notre Dame Radiation Laboratory, Notre Dame, Indiana 46556

Received: July 22, 2004; In Final Form: December 9, 2004

The rate constant for the reaction of hydrogen atoms ($H^•$) with hydroxide ions (OH^-) in aqueous solution has been measured from 100 to 300 °C by direct measurement of the hydrated electron ($(e^-)_{aq}$) product growth rate. In combining these measurements with previous results, the reaction is observed to display Arrhenius behavior in two separate temperature regions, 3−100 and 100−330 °C, where the data above 100 °C show an obvious decrease in activation energy from 38.2 ± 0.6 to 25.4 ± 0.8 kJ mol^{-1}. The value of the rate constant is smaller than that estimated previously in the 200−300 °C range. The very unusual activation energy behavior of the forward and backward reactions is discussed in the context of transition state theory.

I. Introduction

To make predictions of the radiation-induced chemistry in the primary heat transport system of nuclear reactors, it is necessary to understand the kinetics of many important reactions over the range of reactor operating temperatures. In recent years, rate constants for several vital reactions have been determined.[1−6] In our continuing study of high-temperature and pressure water radiation chemistry, we have reexamined the very unusual reaction of the hydrogen atom ($H^•$) with the hydroxide ion (OH^-) in the 100−300 °C temperature range.

The equilibrium process

$$H^• + OH^- \rightleftharpoons (e^-)_{aq} + H_2O \quad (1)$$

is of critical importance in both radiation chemistry and nuclear reactor engineering as it determines the lifetime and limiting concentration of the hydrated electron ($(e^-)_{aq}$) in water. Since both the $H^•$ and hydrated electron free radicals are highly reactive, the equilibrium constant has been determined by separate measurements of the forward[4,7−9] and reverse[10−13] reaction rates. Determination of their temperature dependence has allowed the evaluation of the $(e^-)_{aq}$ solvation thermodynamics.[9,11,14,15]

The equilibrium constant for reaction 1, K_1, can be expressed as

$$K_1 = \frac{k_1}{k_{-1}} = \frac{K_H}{K_w} \quad (2)$$

where k_1 and k_{-1} respectively represent the rate constants for the forward and reverse reactions, K_H is the equilibrium constant for $H^•$ atom ionization,

$$H^• \rightleftharpoons (e^-)_{aq} + H^+ \quad (3)$$

and K_w corresponds to the ionic product for water dissociation

$$H_2O \rightleftharpoons H^+ + OH^- \quad (4)$$

K_w and K_H have been measured from room temperature up to 1000[16] and 250 °C,[15] respectively.[17,18] A polynomial for pK_H has been reported as a function of temperature just above the liquid/vapor coexistence pressure,[19] and ref 16 gives an equation for K_w that includes both its temperature and density dependence. With knowledge of K_w and K_H, values for K_1 can be calculated reliably up to 250 °C. However, knowledge of K_1 as a function of temperature merely defines the temperature dependence of the ratio k_1/k_{-1}, and does not explicitly assign values to either k_1 or k_{-1}.

Previous measurements in this laboratory examined k_1 from room temperature to 98 °C[8,9] and from 200 to 380 °C,[4] demonstrating that the Arrhenius behavior observed below 100 °C cannot be extrapolated to higher temperatures. In the current paper, we have measured k_1 from 100 to 300 °C, filling in the gap where data were missing between 100 and 200 °C and reconfirming the overall non-Arrhenius behavior of the rate constant. We find that the activation energy suddenly decreases near 100 °C. Given prior knowledge of K_1, the rate constant for the back reaction between $(e^-)_{aq}$ and H_2O can also be calculated. Transition state theory is used to explore the thermodynamics of the forward and backward reactions.

II. Experimental Section

Pulse radiolysis/transient absorption experiments were carried out using 4-ns pulses from the Argonne Chemistry Division's

† This is document number NDRL-4565 from the Notre Dame Radiation Laboratory.

* To whom correspondence should be addressed. E-mail: bartels@hertz.rad.nd.edu. Fax: (574) 631-8068.

‡ Current address: Chemistry Department, Benedictine University, Lisle, IL 60532.

10.1021/jp046737i CCC: $30.25
Published on Web 02/12/2005

20-MeV electron linac. The high-temperature/pressure sample cell, flow system, and basic experimental setup and characteristics were described in previous publications.[4,20] Normal temperature and pressure stabilities were ± 0.2 °C and ± 0.1 bar, respectively. Analyzing light from a pulsed 75-W xenon lamp (Photon Technology International) was selected using a 40-nm bandwidth interference filter (Andover Corporation) with a center wavelength corresponding to the maximum absorption of $(e^-)_{aq}$. Because the $(e^-)_{aq}$ absorption spectrum is sensitive to both temperature and density, wavelengths were chosen to coincide with the absorption maximum at each temperature. (The red shift and width of the $(e^-)_{aq}$ spectrum at elevated temperatures will be the subject of a future publication.[21]) A germanium photodiode (GMP566, Germanium Power Devices, Inc.) was used for detection. The inherent biexponential transient response of the photodiode[22] was accounted for in the data fitting as a convolution with the $(e^-)_{aq}$ absorption. Kinetics were measured from 100 to 300 °C in steps of 50 °C. Unfortunately, data could not be acquired at temperatures higher than 300 °C, as significant corrosion began to occur in the sample cell under alkaline, hydrogenated water conditions, altering the $(e^-)_{aq}$ kinetics.

Standardized 0.991 M potassium hydroxide (KOH) solutions (Aldrich, used as received) were diluted to the appropriate concentration in deionized water (18.2 MΩ-cm, Barnstead Nanopure system). Alkaline water samples were kept under nitrogen or argon at all times to avoid contamination by carbonate ions arising from possible carbon dioxide absorption, and were purged with Argon for at least 30 min prior to collecting data. Pressurized hydrogenated water samples were prepared in our laboratory-built gas−liquid saturator. Details of this device have been previously published.[2]

Individual control over the hydrogenated water and KOH solution flow rates was achieved with two separate HPLC pumps (Alltech 301). In all experiments, the hydrogen concentration was kept at a constant 0.024 mol kg^{-1} (m) in the sample cell. Four different KOH solutions were used to give total OH^- concentrations of 1.00×10^{-2}, 4.00×10^{-3}, 1.50×10^{-3}, and 3.00×10^{-4} m in the sample cell (solution concentrations considered reliable within 2%). System total flow rates were generally ∼1.8 mL/min, adjusted as necessary to achieve an experimental pressure of 250 bar.

The radiolysis of water by γ photons, high-energy electrons, neutrons, or recoil ions can be represented by

$$H_2O \xrightarrow{radiation} H^\bullet, OH^\bullet, (e^-)_{aq}, (H^+)_{aq}, H_2O_2, H_2, HO_2 \quad (5)$$

Water radiolysis is kinetically complex, and entails some 50 competing reactions involving the water decomposition species shown above.[19,23] Many of these are second-order recombination reactions, which can be suppressed by carrying out pulsed experiments using low radiation doses. Moreover, in hydrogenated alkaline water, the transient absorption from $(e^-)_{aq}$ can be approximated by just three dominant reactions:

$$H_2 + OH^\bullet \rightarrow H^\bullet + H_2O \quad (6)$$

$$H^\bullet + OH^- \rightleftharpoons (e^-)_{aq} + H_2O \quad (1)$$

$$(e^-)_{aq} + (e^-)_{aq} \rightleftharpoons 2OH^- + H_2 \quad (7)$$

The rate constant for reaction 1 is easily measured by monitoring the growth of $(e^-)_{aq}$, which has a strong absorption in the red and near-infrared spectral regions ($\epsilon_{max} = 18\,400\ M^{-1}cm^{-1}$ at

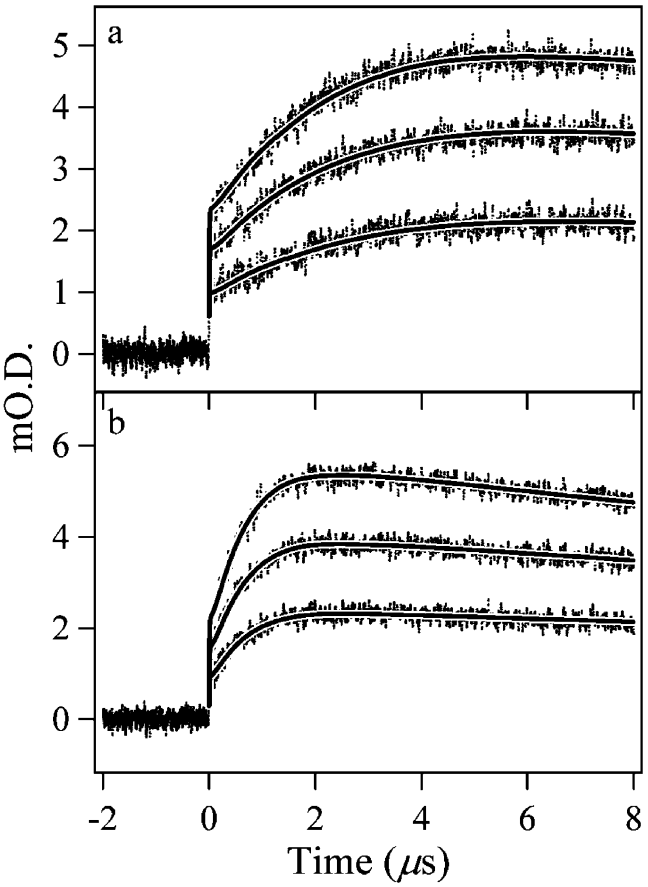

Figure 1. Formation of $(e^-)_{aq}$ at 150 °C and an OH^- concentration of a) 3.00×10^{-4} m and (b) 1.50×10^{-3} m. The signal is acquired at the wavelength peak of the $(e^-)_{aq}$ absorption spectrum. The three traces correspond to three applied radiation doses. Fits to the kinetics are superimposed as solid lines.

room temperature[26]). This growth is followed by a second-order decay arising from reaction 7. At low radiation doses, the second-order decay rate is suppressed, allowing the hydrated electron to live for many tens of microseconds. In the limit of high hydrogen concentration (>0.010 M), reaction 6 becomes fast compared to reaction 1, and thus the growth of $(e^-)_{aq}$ is limited by the rate of reaction 1. Nonetheless, knowledge of the reaction 6 rate constant (k_6) is essential to properly ascertain the reaction 1 rate constant (k_1), especially in the limit of very high OH^- concentrations (∼0.01 M), where the reaction 1 rate approaches that of reaction 6. Values of k_6 were previously determined in our laboratory up to 350 °C.[2]

Since $k_1 \gg k_{-1}$, k_1 can be determined by merely examining the growth rate of $(e^-)_{aq}$, which under conditions of hydrogenated, alkaline water and low doses of radiation, could be described as a first-order growth atop the prompt $(e\text{-})_{aq}$ generated directly by radiolysis (see Figure 1). However, a wide range of OH^- concentrations was used in these studies to ensure confident fits to the reaction 1 rate constant. Over this entire range, the observed pseudo-first-order growth of $(e^-)_{aq}$ is not preserved, as contribution of the reaction 6 rate becomes increasingly important. At the highest OH^- concentrations, the reaction 6 and reaction 1 rates are not well-separated, and therefore the $(e^-)_{aq}$ rise time is no longer purely limited by reaction 1. Furthermore, the intrinsic secondary response of the photodiode[22] used in the experiment coincides with the time scale of the acquired kinetic data, and must be included as an instrument response convolution.

The data were fit using a differential equation model that incorporates all of the known recombination reactions as well as yields of water radiolysis species at high temperature, as assembled by Elliott.[19] High-temperature rate constants for reaction 6 were taken from ref 2. The model is coupled to a fitting routine based on Gauss−Newton minimization, incorporating modifications from the traditional Marquardt−Levenberg approach.[24,25] The program is set up to specifically fit the $(e^-)_{aq}$ kinetics by iterating the reaction rate constants of our choice, while keeping all other (known) parameters fixed.

A sensitivity analysis for all the radiolysis rate constants confirmed that for the radiation doses and OH^- concentrations used in these studies, only k_1, k_6, and k_7 need be examined in detail, as individual changes to other rate constants in the model negligibly affect the fitted k_1 value. Yet, use of the full model and incorporating all the reactions modestly benefits the quality of the fit as a whole, and gives us more confidence that the model is indeed reproducing the experimental data. Rate constants for the remaining reactions were left fixed to the values provided by Elliot.[19] The value of k_6 was also fixed based on its previous determination.[2] The reaction 7 rate constant is known to decrease with increasing temperature over the temperature range considered here, but reliable values of the rate constant are not yet available. (Reaction 7 will be examined in greater detail in the future.) Consequently this parameter was fitted along with k_1. Global fits to k_1 and k_7 were performed over all applied doses for a given temperature and OH^- concentration. The reaction 1 rate exceeds that of reaction 7 by a factor of ~50 so that their rate coefficients are relatively uncorrelated. The fitted values to k_7 are not significant here as a proper determination of k_7 requires data to be acquired on a much longer time scale than used in these measurements. Nonetheless, fitted values at lower temperatures were within ~35% of rate constant values previously reported.[26]

Because the χ^2 surface for this system of equations is not quadratic, the least-squares standard deviation does not provide a meaningful error estimate.[24,25] The χ^2 surface of the system was mapped out by changing and fixing the value of each parameter near its optimum value, then reoptimizing all other parameters. The change needed to double χ^2 is a reasonable estimate of the error in the fitted parameter, so long as two parameters do not have very large covariance. In all cases this error is well below 10% and no large covariance is observed. We take 10% as a conservative estimate of the rate constant uncertainties, rather than reporting the entire analysis.

III. Results and Discussion

Typical data taken at 150 °C and OH^- concentrations of 3.0×10^{-4} m and 1.5×10^{-3} m are shown in Figure 1, with fitted curves superimposed. The data reflect the growth of $(e^-)_{aq}$ at 900 nm, and the three different traces acquired at each concentration correspond to three applied doses. The subsequent decay of $(e^-)_{aq}$ due to reaction 7 occurs on a time scale of tens of microseconds in all cases, and was not examined in these experiments. Applied doses generated $(e^-)_{aq}$ concentrations of $\sim(20-130) \times 10^{-9}$ m. As expected from pseudo-first-order behavior, an increase in OH^- concentration gives an increase in the growth rate of $(e^-)_{aq}$. Fitted values of k_1 as a function of temperature are given in Table 1.

An Arrhenius plot of k_1 is shown in Figure 2 (squares) alongside data previously reported. Triangles indicate low-temperature data acquired from pulse radiolysis/EPR and optical spectroscopy[8,9] and circles indicate high-temperature data acquired from pulse radiolysis/optical spectroscopy.[4] The new data slightly undershoot previous results over the 200−300 °C temperature range. (Below 300 °C, $H^\bullet$ atoms account for less than 20% of the total radiolysis yield, giving weak experimental signals in the previous study. Above 300 °C, the $H^\bullet$ atom yield rapidly increased, allowing reliable measurements in this range. The quality of the current data is not so dependent on the initial $H^\bullet$ atom yield.) On the basis of our fitting sensitivity analysis, we can confidently report that errors in the fitted k_1 values are <10% at every temperature, whereas previous errors were up to ~ 50% at 200 °C. Note that at 300 °C and above, where the $H^\bullet$ atom yield becomes sizable, the data agree within 20%. The solid lines in Figure 2 represent Arrhenius fits in the 3−98 °C and 100−330 °C temperature ranges, where the latter incorporates two previously obtained data points at 328 and 330 °C. Data at still higher temperatures and lower density do not show the same Arrhenius behavior[4] and consequently are not included in the Arrhenius fits. Compared to the low-temperature data, current results exhibit a smaller activation energy. An Arrhenius fit to data from 100 to 330 °C gives an activation energy of 25.4 ± 0.8 kJ mol^{-1} and a prefactor of $1.76 \pm 0.36 \times 10^{12}$ M^{-1} s^{-1}, where previous low-temperature results gave values

TABLE 1: Values of the Reaction 1 Rate Constant as a Function of Temperature, Acquired from Global Fits to the $(e^-)_{aq}$ Kinetics at Each Temperature and OH^- Concentration[a]

temperature (°C)	rate constant k_1 (M^{-1} s^{-1})
100	5.01×10^8
150	1.34×10^9
200	2.79×10^9
250	4.76×10^9
300	8.59×10^9

[a] Uncertainties are ±10%.

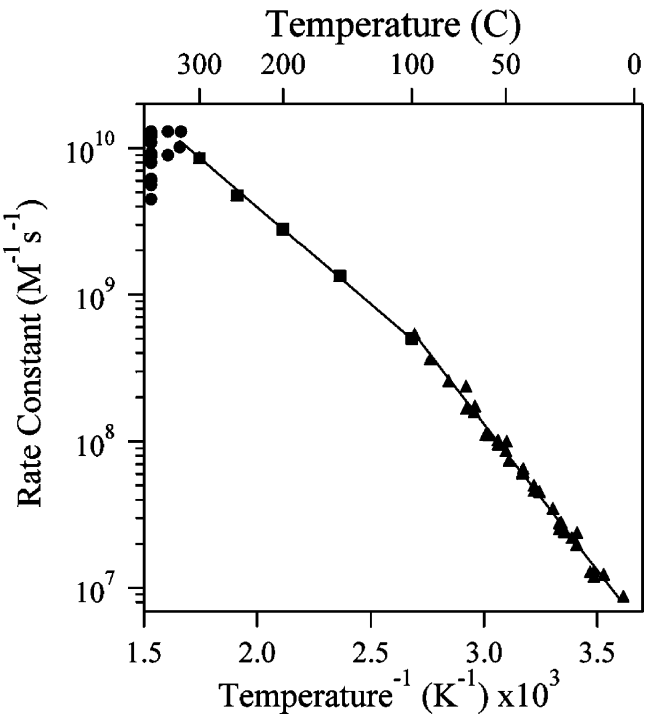

Figure 2. Arrhenius plot for the reaction 1 rate constant k_1. Three sets of data are presented: current data (squares), previous low-temperature data acquired from pulse radiolysis/EPR and optical spectroscopy (triangles) and high-temperature data acquired from pulse radiolysis/optical spectroscopy (circles). Error bars for the current data are on the order of the point size. Arrhenius fits (solid lines) to regions above and below 100 °C are shown by solid lines.

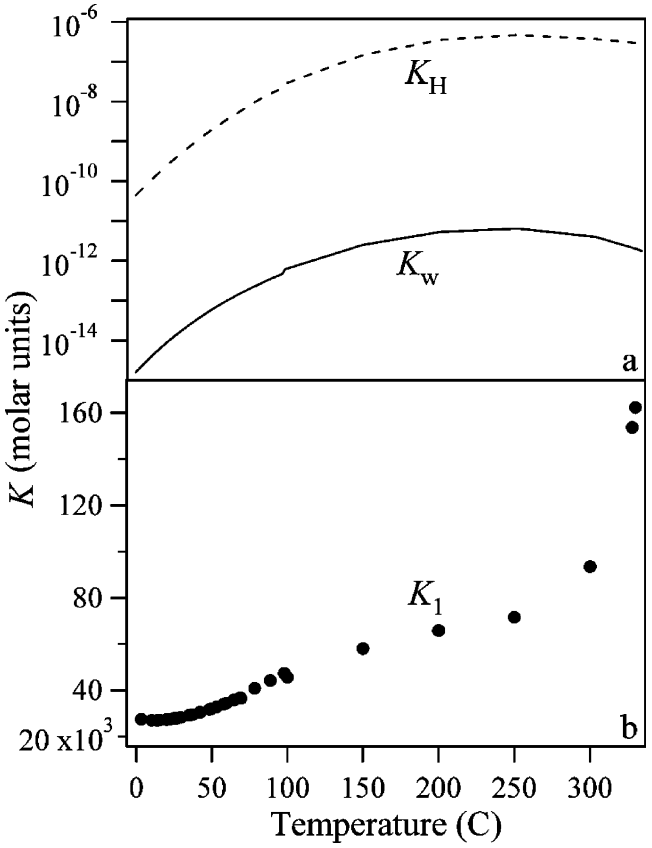

Figure 3. Temperature dependence of equilibrium constants: (a) K_H (dashed line) and K_w (solid line), (b) K_1. The ~ 30% increase observed at 100 °C for K_H and K_w is due to data acquisition at two different pressures. Note that the *y*-axis for panel a is a log scale and that for panel b is a linear scale.

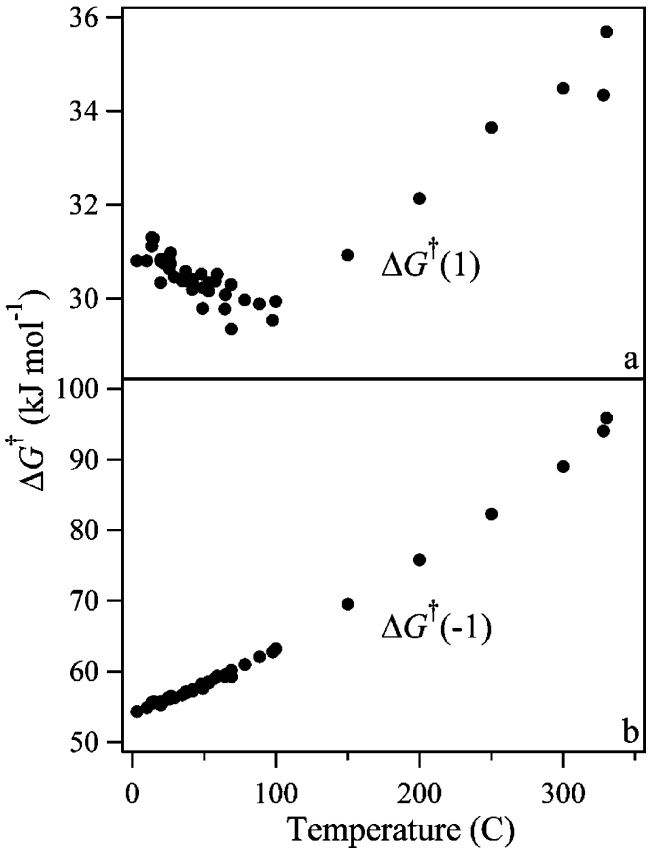

Figure 4. Temperature dependence of the Gibbs free energy of activation as acquired via transition state theory for (a) reaction 1 and (b) reaction −1.

of 38.2 ± 0.6 kJ mol^{-1} and 1.27 ± 0.27 × 10^{14} M^{-1} s^{-1}, respectively.

Figure 3 shows (a) K_w, K_H, and (b) K_1 as a function of temperature, given the pressures specifically used in our experiments. It was noted by Shiraishi et al.[15] that K_H closely parallels the temperature dependence of K_w because both equilibria involve a neutral molecule dissociating into ions. In Figure 3, K_w and K_H suddenly increase by 30% at 100 °C because the data below this temperature were obtained at 1 bar pressure, whereas those above 100 °C were acquired at 250 bar. Available data from the water ionic product dictates this increase for higher densities. Although pressure-dependent data are not available for K_H, the same trend as for K_w is assumed. The available K_H data[15] were acquired near the water gas/liquid coexistence pressure (p_{coex}). Since our data were collected at a pressure of 250 bar, we multiply the molal K_H values by the ratio K_w(250 bar)/K_w(p_{coex}) to add a small K_H density correction. Values of K_H at p_{coex} above 250 °C are extrapolated using Shiraishi's equation.[15] The plot shows that K_1 is relatively insensitive to temperature, and at the lowest OH^- concentration used in these experiments (3.00 × 10^{-4} m), the equilibrium ratio of the concentrations of $(e^-)_{aq}$ to $H^\bullet$ should be in the range of 450−1200, allowing direct determination of k_1.

On the basis of the K_1 values, the rate constant for the reverse of reaction 1 (k_{-1}) can be obtained via eq 2. Again, Arrhenius fits can be performed on two regions of data above and below 100 °C with different activation energies, though in this case the cause of the change at 100 °C is merely the implicit dependence of k_{-1} on k_1 as we have calculated it here. A fit to the data from 100 to 330 °C gives an activation energy of 22.1 ± 1.3 kJ mol^{-1} and a prefactor of 2.61 ± 0.83 × 10^5 s^{-1}, where below 100 °C these parameters are 33.1 ± 0.6 kJ mol^{-1} and 5.84 ± 1.41 × 10^8 s^{-1}, respectively.

Following the standard methods of transition state theory,[27] a measured rate constant can be represented by

$$k = \frac{\kappa k_B T}{c_o h} \exp\left(-\frac{\Delta G^\dagger}{RT}\right) \quad (8)$$

where k_B is Boltzmann's constant, h is Planck's constant, R is the gas constant, T is temperature in K, c_o (=1 M) is the ratio of standard state concentrations for the transition state/reactant equilibrium,[28] and $\Delta G^\dagger$ is the difference in free energy between the transition state and reactants. We follow the usual assumption that all species reaching the transition state irreversibly form product and therefore set the transmission coefficient κ to unity. The free energy of activation breaks down into the entropy (S) and enthalpy (H) of activation via $\Delta G^\dagger = \Delta H^\dagger - T\Delta S^\dagger$. Thus, with rate constants in hand, $\Delta G^\dagger$ can be obtained for both the forward and reverse of reaction 1, and $\Delta H^\dagger$and $\Delta S^\dagger$ can also be obtained.

Figure 4 shows the temperature dependence of $\Delta G^\dagger$ for the forward and reverse reactions, respectively. Note that $\Delta G^\dagger$ for the forward reaction ($\Delta G^\dagger(1)$) is fairly temperature-insensitive, changing by only ~6 kJ mol^{-1} over the entire temperature range, whereas $\Delta G^\dagger$ for the backward reaction ($\Delta G^\dagger(-1)$) changes significantly, increasing by ~ 48 kJ mol^{-1}. The forward reaction is dominated by enthalpy, while the back reaction has a large entropy component. The most curious aspect of the activation thermodynamics is the sudden change in the slope of $\Delta G^\dagger(1)$ at about 100 °C. Nominally the activation entropy of reaction 1 changes sign from positive to negative at this point. At 25

°C, $\Delta H^{\dagger}$ and $\Delta S^{\dagger}$ have values of 35.7 kJ mol^{-1} and +16.8 J mol^{-1}K^{-1} respectively, whereas at 100 °C these values are 22.3 kJ mol^{-1} and −20.6 J mol^{-1}K^{-1}. It is straightforward to add additional temperature dependence to the thermodynamics by fitting $\Delta G^{\dagger}(1)$ with a ΔC_p term, as was done by Shiraishi et al.[15] for the equilibrium. However, since the temperature dependence of $\Delta G^{\dagger}(1)$ is not quadratic (see Figure 4), this yields unphysically large values for ΔC_p and still does not give reasonable fits, given the very sudden change in slope of $\Delta G^{\dagger}$ for reaction 1.

It is unclear why there should be two separate Arrhenius regions for reaction 1. The properties of water and the solvent structure are not dramatically changing in this temperature range. The experimental pressure change between 98 and 100 °C should not have greatly affected the thermodynamics. This leads us to examine in more detail the assumptions we have made in applying transition state theory to the problem.

A first basic assumption is that we are dealing with a single elementary reaction with a transition state bottleneck, and not with a short-lived intermediate and a back reaction. In the latter case, reaction 1 would actually be a consecutive process with two rate constants determining the overall reaction rate such as

$$H^{\bullet} + OH^{-} \overset{k_a}{\rightleftharpoons} \text{intermediate} \overset{k_b}{\rightleftharpoons} (e^{-})_{aq} + H_2O \qquad (9)$$

Assuming different Arrhenius parameters for each step of the reaction, it is possible that the rate-determining step of the reaction is dependent on the temperature and k_b could become less than k_a at 100 °C. One might imagine that the excess electron becomes localized on an intermediate of the form H_2O^{-}, which then splits to give the H$^{\bullet}$ and OH^{-} products. However, this possibility was considered in a previous publication and dismissed for the temperature range below 100 °C because of the equivalence of EPR and optical reaction rates.[9] An intermediate allowing the exchange of protons would be detected as an additional spin relaxation rate in the EPR experiment. Perhaps this EPR experiment should be repeated for higher temperatures, but the existence of a short-lived intermediate seems very unlikely.

A second assumption is in setting the transmission coefficient, κ, equal to unity, independent of temperature. This factor accounts for both the possibilities of quantum mechanical tunneling and for the contributions of solvent friction. At lower temperatures, tunneling can be essentially ruled out experimentally. Previous experiments showed absolutely no kinetic isotope effect when H$^{\bullet}$ in reaction 1 was replaced by deuterium[9] in measurements up to 100 °C, and at most a ∼ 30% isotope effect exists between H$^{\bullet}$ atom and the unstable light isotope muonium, where muonium shows a higher rate constant above 100 °C,[29,30] but lower below 100 °C.[31] The reaction enthalpy is overall positive, so in general there is no place at lower energy on the barrier for the H$^{\bullet}$ atom to tunnel toward. The small apparent muonium isotope effect then could be assigned to energy differences of the reactants, i.e., zero point[32] and solvation energies.[33] Another scenario to give κ a value less than unity is the contribution of temperature or pressure-dependent Kramers[34] or Grote−Hynes[35] type solvent friction. This could conceivably vary over the temperature range studied due to physical rearrangements in the water solvent and changes in its properties. One would have to postulate a greater friction at higher temperature. However, this behavior should tend to cause the heavier isotope to have the larger rate constant.

Finally, we have also made the assumption that semiclassical transition state theory applies to the reaction. If the reaction actually involves nonadiabatic transitions between coupled proton and electron states, the simple $\kappa k_B T/c_0 h$ prefactor will no longer apply. In this case a quantum treatment might be applied to the proton transfer,[36,37] or a Marcus-type theory with a Fermi golden rule rate expression could be more appropriate.[38,39] As we are unable to qualitatively explain the rate constant result via (adiabatic) transition state theory, we lean toward this (nonadiabatic) explanation, and invite others to take up the challenge of elucidating the reaction mechanism.

Acknowledgment. We thank Dr. Sergey Chemerisov for maintaining and operating the linac accelerator used in this work. We are grateful to Dr. Khashayar Ghandi, Prof. Paul W. Percival, and Prof. Sharon Hammes-Schiffer for helpful discussions. Work at Argonne National Laboratory and at Notre Dame Radiation Laboratory was performed under US-DOE Nuclear Energy Research Initiative Grant M2SF02-0060.

References and Notes

(1) Takahashi, K. J.; Ohgami, S.; Koyama, Y.; Sawamura, S.; Marin, T. W.; Bartels, D. M.; Jonah, C. D. *Chem. Phys. Lett.* **2004**, *383*, 445−450.

(2) Marin, T. W.; Bartels, D. M.; Jonah, C. D. *Chem. Phys. Lett.* **2002**, *371*, 144−149.

(3) Marin, T. W.; Cline, J. A.; Bartels, D. M.; Jonah, C. D.; Takahashi, K. *J. Phys. Chem. A* **2002**, *51*, 12270−12279.

(4) Cline, J. A.; Takahashi, K.; Marin, T. W.; Jonah, C. D.; Bartels, D. M. *J. Phys. Chem. A* **2002**, *106*, 12260−12269.

(5) Lundstrom, T.; Christensen, H.; Sehested, K. *Radiat. Phys. Chem.* **2004**, *69*, 211−216.

(6) Lundstrom, T.; Christensen, H.; Sehested, K. *Radiat. Phys. Chem.* **2002**, *64*, 29−33.

(7) Matheson, M. S.; Rabani, J. *J. Phys. Chem.* **1965**, *69*, 1324−1335.

(8) Han, P.; Bartels, D. M. *J. Phys. Chem.* **1990**, *94*, 7294−7299.

(9) Han, P.; Bartels, D. M. *J. Phys. Chem.* **1992**, *96*, 4899−4906.

(10) Fielden, E. M.; Hart, E. J. *Trans. Faraday Soc.* **1967**, *63*, 2975−2982.

(11) Schwarz, H. A. *J. Phys. Chem.* **1992**, *96*, 8937−8941.

(12) Swallow, A. J. *Photochem. Photobiol.* **1968**, *7*, 683−694.

(13) Hart, E. J.; Gordon, S.; Fielden, E. M. *J. Phys. Chem.* **1966**, *70*, 150−156.

(14) Jortner, J.; Noyes, R. M. *J. Phys. Chem.* **1966**, *70*, 770−774.

(15) Shiraishi, H.; Sunaryo, G. R.; Ishigure, K. *J. Phys. Chem.* **1994**, *98*, 5164−5173.

(16) Marshall, W. L.; Franck, E. U. *J. Phys. Chem. Ref. Data* **1981**, *10*, 295−304.

(17) The water solvent is taken to have unit activity at all temperatures and pressures. The density of water changes as a function of temperature, decreasing approximately 25% over the range 100−300 °C. Thus, the K_H molal equilibrium constant is multiplied by the water density (in kg L^{-1}) and the K_w molal ionic product is multiplied by the water density squared to convert to molar units. This ensures consistency of units between our reported equilibrium constants and rate constants. Corrections for changes in the water concentration as a function of temperature are obtained from the water equation of state, given in ref 18.

(18) Wagner, W.; Kruse, A. *Properties of Water and Steam*; Springer-Verlag: Berlin, 1998.

(19) Elliot, A. J. Rate Constants and G-Values for the Simulation of the Radiolysis of Light Water over the Range 0−300 °C. AECL, 1994.

(20) Takahashi, K.; Cline, J. A.; Bartels, D. M.; Jonah, C. D. *Rev. Sci. Instrum.* **2000**, *71*, 3345−3350.

(21) Bartels, D. M.; Takahashi, K.; Cline, J. A.; Marin, T. W.; Jonah, C. D. *J. Phys. Chem. A.*, in press.

(22) Cline, J. A.; Jonah, C. D.; Bartels, D. M. *Rev. Sci. Instrum.* **2002**, *73*, 3908−3915.

(23) Draganic, I. G.; Draganic, Z. D. *The Radiation Chemistry of Water*; Academic Press: New York, 1971.

(24) Levenberg, K. *Q. Appl. Math.* **1944**, *2*, 164−168.

(25) Press, W. H.; Flannery, B. P.; Teukolsky, S. A.; Vetterling, W. T. *Numerical Recipes*, 2nd ed.; Cambridge University Press: Cambridge, England, and New York, 1992.

(26) Christensen, H.; Sehested, K. *J. Phys. Chem.* **1986**, *90*, 186.

(27) Steinfeld, J. I.; Francisco, J. S.; Hase, W. L. *Chemical Kinetics and Dynamics*; Prentice Hall: Englewood Cliffs, NJ, 1989.

(28) Robinsion, P. J. *J. Chem. Educ.* **1978**, *55*, 509−510.

(29) Ghandi, K.; Addison-Jones, B.; Brodovitch, J. C.; Kecman, S.; McKenzie, I.; Percival, P. W. *Physica B* **2003**, *326*, 55−60.

(30) Ghandi, K. Muonium Chemistry in Sub and Supercritical Water. Thesis, Simon Fraser University, 2002.
(31) Ng, B. W.; Stadlbauer, J. M.; Walker, D. C. *J. Phys. Chem.* **1984**, *88*, 857−860.
(32) Roduner, E.; Percival, P. W.; Han, P.; Bartels, D. M. *J. Chem. Phys.* **1995**, *102*, 5989−5997.
(33) Gai, H. D.; Garrett, B. C. *J. Phys. Chem.* **1994**, *98*, 9642−9648.
(34) Kramers, H. A. *Physica (The Hague)* **1940**, *7*, 284−304.
(35) Grote, R. F.; Hynes, J. T. *J. Chem. Phys.* **1980**, *73*, 2715−2732.
(36) Hammes-Schiffer, S. *Acc. Chem. Res.* **2001**, *34*, 273−281.
(37) Kim, S. Y.; Hammes-Schiffer, S. *J. Chem. Phys.* **2003**, *119*, 4389−4398.
(38) Brunschwig, B. S.; Sutin, N. *Commun. Inorg. Chem.* **1987**, *6*, 209−235.
(39) Bixon, M.; Jortner, J. Electron Transfer − From Isolated Molecules to Biomolecules. In *Electron Transfer-From Isolated Molecules to Biomolecules, Part 1*; Advances in Chemical Physics, Vol. 106; Wiley: New York, 1999; pp 35−202.